Journal of Power Sources 236 (2013) 87–94

Contents lists available at SciVerse ScienceDirect

Journal of Power Sources

journal homepage: www.elsevier.com/locate/jpowsour

Influence of the carbonaceous conductive network on the electrochemical performance of $ZnFe_2O_4$ nanoparticles

Franziska Mueller, Dominic Bresser*, Elie Paillard, Martin Winter, Stefano Passerini*

Institute of Physical Chemistry & MEET Battery Research Centre, University of Muenster, Corrensstr. 28/30 & 46, 48149 Muenster, Germany

HIGHLIGHTS

- Realization of carbonaceous percolating networks incorporating $ZnFe_2O_4$ nanoparticles.
- Reduced surface film formation by homogenous carbon coating of $ZnFe_2O_4$ nanoparticles.
- Sucrose as carbon precursor grants enhanced electrochemical performance of $ZnFe_2O_4$.

ARTICLE INFO

Article history:
Received 6 December 2012
Received in revised form
2 February 2013
Accepted 13 February 2013
Available online 26 February 2013

Keywords:
$ZnFe_2O_4$
Carbon coating
Carbon precursor
Anode
Lithium-ion battery

ABSTRACT

Herein, the influence of the carbon precursor used for the realization of carbonaceous percolating network incorporating $ZnFe_2O_4$ is investigated. Three different precursors, namely sucrose (Suc), citric acid (CA), and oleic acid (OLEA) were used for the realization of such carbonaceous matrix. The composite materials were characterized by means of thermogravimetric analysis (TGA), gas adsorption using the BET isotherm, Raman spectroscopy, X-ray diffraction (XRD), and scanning electron microscopy (SEM). Electrodes based on the resulting composite materials were investigated, performing electrochemical impedance spectroscopy and galvanostatic cycling. The results showed that the homogeneity of the carbon coating rather than the absolute amount of carbon enhanced the electrochemical performance of $ZnFe_2O_4$ nanoparticles. The most advantageous coating properties were obtained with sucrose as carbon precursor, obtaining a highly stable specific capacity higher than 1000 mAh g^{-1} for more than 60 cycles.

1. Introduction

Due to the steadily increasing worldwide demand for energy and the limited resources of fossil fuels such as crude oil, coal, and natural gas, renewable energy technologies are gathering increasing attention by scientific researchers and politicians. Nonetheless, the efficient utilization of renewable energy is strongly correlated to the identification of suitable storage devices. Particularly with respect to modern transportation, as *inter alia* cars, alternatives to the classical combustion engine are required in order to enable the use of renewable energy for future society's mobility. One possible and currently most likely considered alternative is the electric vehicle (EV), based on the utilization of a battery as energy and power supply. However, beside low cost, high reliability, and high safety, the desired battery should offer low overall weight and volume. One of the most promising candidates to fulfill these requirements is certainly the lithium-ion battery (LIB), as it offers superior gravimetric and volumetric energy and power densities, highly efficient energy conversion, and long battery life altogether [1,2]. Nevertheless, further improvement of the existing lithium-ion technology is required in order to enhance the energy and power density as well as safety.

Carbonaceous anode materials, as one component of the battery, suffer from safety issues due to the low lithiation potential and the accompanied risk of metallic lithium deposition as well as the comparatively low theoretical capacity (e.g. 372 mAh g^{-1} for graphite). $ZnFe_2O_4$ (ZFO) has attracted increasing interest as alternative, promising new anode material due to its attractive theoretical specific capacity of more than 1000 mAh g^{-1}. Furthermore, it is environmentally friendly, non-toxic, as well as based on abundant elements and thus cheap. The major challenge for ZFO-based anodes is the observed capacity fading upon cycling and a poor high rate capability [3–7]. Very recently, however, it has been reported that the application of a carbon coating appears to be a very promising approach to overcome these challenges. Carbon coated ZFO electrodes revealed a stable capacity for more than 100 cycles and a significantly enhanced power performance [8].

* Corresponding authors.
E-mail addresses: dominic.bresser@uni-muenster.de (D. Bresser), stefano.passerini@uni-muenster.de (S. Passerini).

0378-7753/$ – see front matter © 2013 Elsevier B.V. All rights reserved.
http://dx.doi.org/10.1016/j.jpowsour.2013.02.051

The effect of a carbon coating on the overall electrochemical performance is strongly correlated to its structural and morphological properties such as uniformity, thickness, relative weight to the coated active material, structure (sp^3 to sp^2 ratio), as well as the carbon precursor source [9–14]. For LTO/carbon composites and LFP/carbon composites, for instance, it was already shown that there is an optimal carbon content and coating layer thickness, for which the electrochemical performance is best [9,12].

Hence, three well established carbon precursors, namely sucrose (Suc), citric acid (CA), and oleic acid (OLEA), were utilized to carbon coat nanosized ZFO [8,9,15–17]. The resulting ZFO/C materials were morphologically and structurally characterized. Subsequently, electrodes based on the composites were investigated performing electrochemical impedance spectroscopy and galvanostatic cycling.

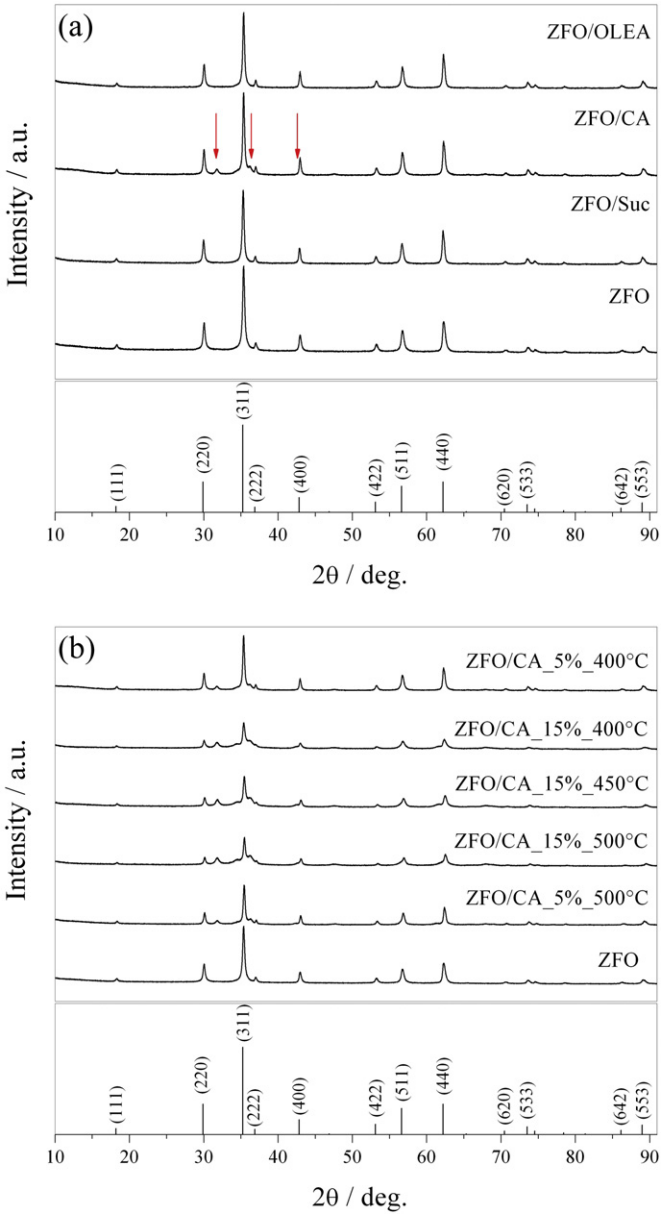

Fig. 1. XRD patterns of (a) pristine ZFO, ZFO/Suc, ZFO/CA, and ZFO/OLEA and (b) pristine ZFO and ZFO/CA with different annealing temperatures and residual carbon content (from bottom to top: ZFO/CA_5%_500 °C, ZFO/CA_15%_500 °C, ZFO/CA_15%_450 °C, ZFO/CA_15%_400 °C, ZFO/CA_5%_400 °C). As reference given in the bottom: JCPDS card no. 00-022-1012.

Table 1
Residual carbon content and specific surface area of pristine ZFO, ZFO/Suc, ZFO/CA, and ZFO/OLEA.

Sample	Residual carbon content [wt.%]	BET surface area [m^2g^{-1}]
ZFO		20.7
ZFO/Suc	16.6	82.6
ZFO/CA	5.4	33.4
ZFO/OLEA	2.2	25.1

2. Experimental

2.1. Preparation and characterization of ZFO/C

Carbon coated ZFO nanoparticles (ZFO/C) were obtained by dispersing 1 g of the as received ZFO (<100 nm, Aldrich Chemistry) either in 1.5 mL of an aqueous carbon precursor solution of Suc (ACROS ORGANICS) or CA (Grüssing) or directly in the liquid carbon precursor OLEA (AppliChem), followed by an annealing step under inert gas atmosphere. The weight ratios were 1:0.75 for ZFO:Suc, 1:1.1 for ZFO:CA, and 1:1.5 for ZFO:OLEA. The obtained dispersions were homogenized by means of a planetary ball mill (Vario-Planetary Mill Pulverisette 4, FRITSCH, 2× 45 min at 400–800 rpm with 10 min rest in between). In order to remove the excess of OLEA a minimum of ethanol was added. The mixture was then centrifuged and the liquid phase comprising the ethanol and the excess OLEA was removed analogous to a method previously reported [18]. Subsequently, the residue (ZFO/OLEA) and the dispersions (ZFO/Suc and ZFO/CA) were dried at 70 °C under ambient atmosphere. After grinding the resulting powders, the composites were annealed in a tubular furnace (R50/250/12, Nabertherm) at 450 °C (ZFO/Suc) and 500 °C, 450 °C or 400 °C (ZFO/CA) for 4 h under a constant argon gas stream. The heating rate was set to 3 °C min^{-1}. The annealing procedure of the ZFO/OLEA residue was slightly different in order to minimize evaporation of OLEA during the heat treatment. In a first step, the temperature was increased to 380 °C with a heating rate of 10 °C min^{-1} and held constant for 30 min. Subsequently, the temperature was further increased with a heating rate of 3 °C min^{-1} to 450 °C and kept constant for 4 h. Higher temperatures were not investigated as Ayyappan et al. [19] have reported a reduction of OLEA capped ZFO under argon at temperatures higher than 480 °C. Prior to their further use, all powders were manually ground in a mortar again.

To determine the residual carbon content, thermogravimetric analysis (TGA) under oxygen atmosphere was carried out (TA

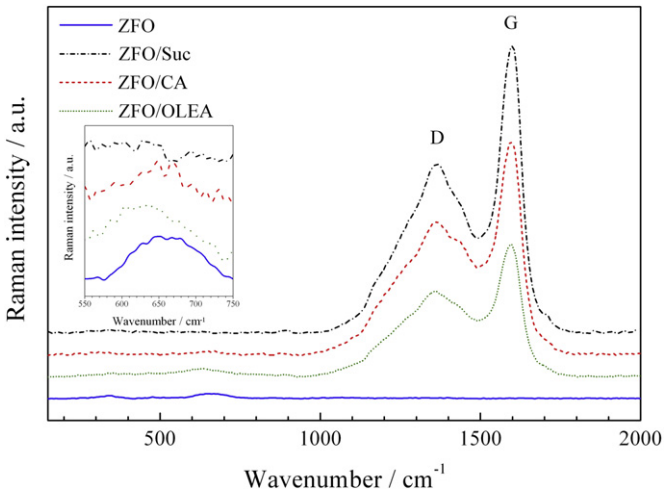

Fig. 2. Raman spectra of pristine ZFO, ZFO/Suc, ZFO/CA, and ZFO/OLEA. Laser wavelength: 532 nm.

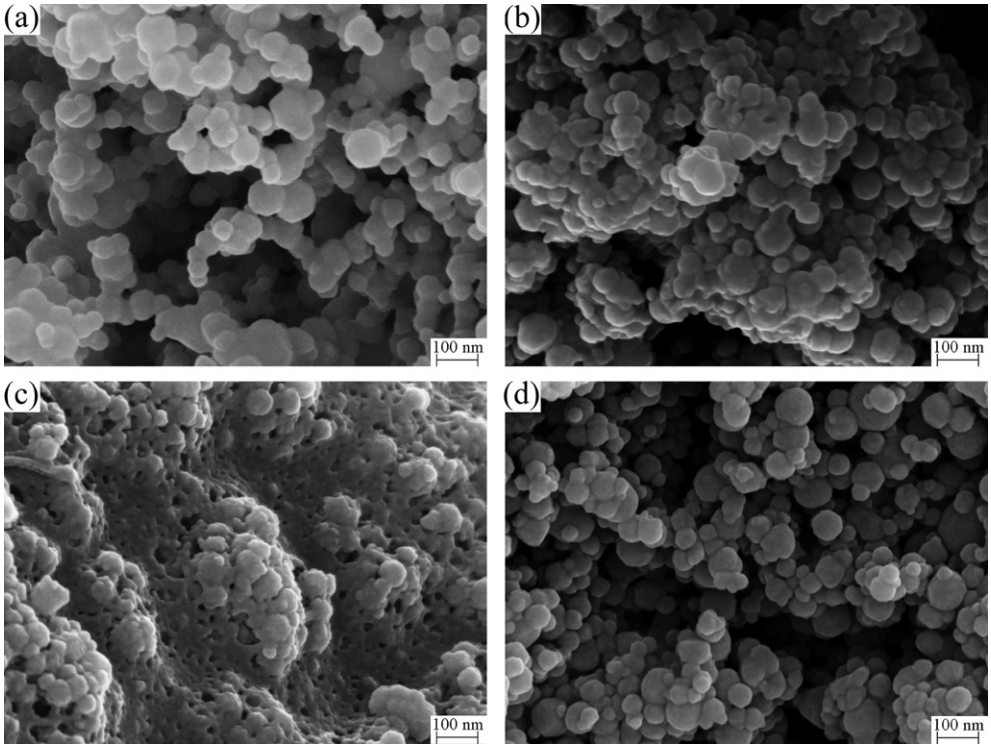

Fig. 3. SEM images of (a) pristine ZFO and carbon coated ZFO: (b) ZFO/Suc, (c) ZFO/CA, and (d) ZFO/OLEA. Magnification: 100 k×.

Instruments Q 5000). The preservation of the phase purity and crystal structure of ZFO after the carbon coating process was confirmed by X-ray diffraction (XRD, Bruker D8 Advance equipped with a copper X-ray tube Cu-$K_{\alpha 1}$ radiation, $\lambda = 154.06$ pm). The homogeneity of the carbon coating was investigated by means of Raman spectroscopy (Bruker Optics Senterra) using a laser with a wavelength of 532 nm and a power of 10 mW. The specific surface area of the different samples has been determined by nitrogen adsorption measurements and calculated according to the Brunauer–Emmett–Teller (BET) method (Micrometrics ASAP 2020). In order to investigate the morphology and surface structure of the samples, high resolution scanning electron microscopy (HRSEM) was performed (Carl Zeiss Auriga® HRSEM). The samples were sputtered with gold for 50 s at 20 mA by means of a sputter coater (Quorum Technologies PQ150T ES).

2.2. Electrode preparation

The electrode coating started with the preparation of slurries containing the active material, the conductive carbon, and the binding agent in a weight ratio of 75:20:5. For this purpose, the binder material (sodium carboxymethylcellulose, CMC, DOW WOLFF CELLULOSICS) was dissolved in ultrapure water. Subsequently, the active material and the conductive agent (carbon black, Super C65®, TIMCAL) were added to the aqueous solution. The obtained mixture was homogenized in a planetary ball mill (Vario-Planetary Mill Pulverisette 4, FRITSCH), using the following mixing procedure: 4× 30 min at 400–800 rpm and 10 min rest in between. After milling, the slurries were immediately casted on dendritic copper foil (SCHLENK) using a laboratory-scale doctor blade. The wet thickness was set to 120 μm. The slurries were dried for 10 min in an oven at 80 °C and then over night at room temperature. Subsequently, electrodes with a diameter of 12 mm were punched and dried under vacuum at 120 °C for around 24 h. The active material mass loading of the electrodes ranged from 1.6 to 2.4 mg cm^{-2}.

2.3. Electrochemical characterization

The electrochemical characterization was performed in three-electrode Swagelok® cells using lithium foil (battery grade, Rockwood Lithium) as counter and reference electrode. All cells were assembled in a glove box (MBraun UNIlab), having a H_2O content <0.5 ppm and an O_2 content <0.5 ppm, under argon atmosphere. The separator (Freudenberg FS 2226) was saturated with the electrolyte comprised of 1 M $LiPF_6$ in a 3:7 volume mixture of ethylene carbonate and diethyl carbonate (UBE). Prior to characterization, the cells were aged for 24 h. Galvanostatic cycling was carried out by means of a Maccor Battery Tester 4300 at 20 ± 1 °C. For the calculation of the C rate a theoretical capacity of 1000 mAh g^{-1} was assumed (1C ≙ 1000 mA g^{-1})based on the theoretical up-take of 9 lithium per formula unit ZFO according to Bresser et al. [8]:

$$ZnFe_2O_4 + 9\ Li^+ + 9\ e^- \rightarrow LiZn + 2\ Fe^0 + 4\ Li_2O$$

The impedance of the investigated electrochemical cells was measured after ten cyclic sweeps at a potential of 3.0 V by means of a Solartron 1260 impedance analyzer connected to a Solartron 1287A potentiostat. The frequency range was set from 100 μHz to 500 kHz with an amplitude of 10 mV. The impedance of cells after certain number of cyclic sweeps was determined utilizing a VMP 3 potentiostat (BioLogic).

3. Results and discussion

The XRD pattern of the as received ZFO nanoparticles, presented in Fig. 1(a and b), is in good agreement with the standard reference (JCPDS card No. 00-022-1012) for the face-centered cubic spinel structure of franklinite ZFO, having the space group *Fd-3m*. No additional reflections were observed, revealing the starting material as phase-pure. The XRD patterns of ZFO/Suc and ZFO/OLEA (Fig. 1a) are as well in good accordance with those of the JCPDS reference and

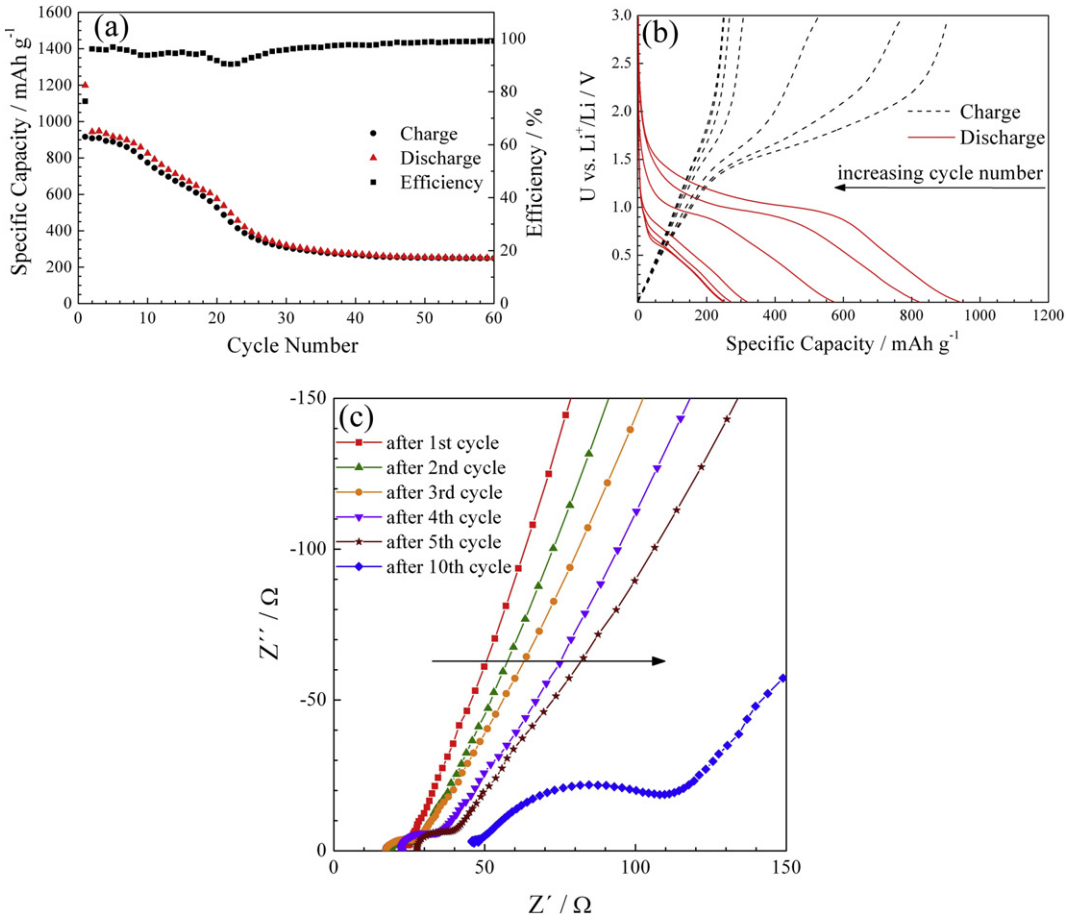

Fig. 4. Electrochemical investigation of electrodes based on pristine ZFO. (a) Galvanostatic cycling. Three formation cycles at C/20 (50 mA g^{-1}), followed by constant current cycling at C/10 (100 mA g^{-1}). Cut-off potentials: 0.01 V and 3.0 V. (b) Potential profiles of the 2nd (C/20), 10th, 20th, 30th, 40th, 50th, and 60th cycle. Cut-off potentials: 0.01 V and 3.0 V. Applied C rate: C/10 (100 mA g^{-1}). (c) Nyquist plots after the 1st, 2nd, 3rd, 4th, 5th, and 10th cyclic potentiodynamic sweep at a potential of 3.0 V.

pristine ZFO, indicating no structural changes upon the carbon coating procedure. As shown in Fig. 1b ZFO/CA composites prepared with different CA amounts and annealed at different temperatures showed additional reflections at 32°, 36°, and 42° which could be assigned to hexagonal ZnO (JCPDS card No. 01-070-8070) and wuestite structured FeO (JCPDS card No. 01-089-0687). A similar reduction behavior was recently reported for OLEA capped ZFO nanoparticles (ø ≈ 10 nm) [19]. It was suggested that upon carbonization the evolving carbon monoxide (CO) reduces the ZFO particles by removing oxygen from the lattice, resulting in the formation of ZnO and FeO [19]. According to the Boudouard equilibrium, the formation of reductive CO is favored at high temperatures, while at lower temperatures the formation of carbon and CO_2 is preferred. However, a further decrease of the temperature to below 400 °C was not investigated, as such a low temperature would no longer guarantee the complete carbonization of CA. It is assumed that an increased formation of CO upon the carbonization process is responsible for the reduction of the ZFO particles, originating from relatively higher oxygen content of CA compared to the other carbon precursors. Nevertheless, the sample ZFO/CA_5%_400 °C, showing the lowest intensity of the impurity reflections, was chosen for the subsequent comparison and subjected to further morphological and electrochemical characterization. Moreover, it should be noted that additional reflections due to carbon could not be detected for any of the samples, thus indicating an amorphous structure of the remaining carbon.

The actual carbon content values detected by TGA-DTG, are given in Table 1. For ZFO/Suc a carbon content of 16.6 wt.% was detected. This value was selected according to previous results of Bresser et al. [8]. The carbon content for the ZFO/CA having the optimal crystallinity was 5.4 wt.%. Due to the more challenging coating procedure, no higher carbon content than 2.2 wt.% could be obtained for ZFO/OLEA.

Raman spectroscopy was performed in order to further evaluate the structure and homogeneity of the applied carbon coating. The resulting spectra are presented in Fig. 2. Compared to pristine ZFO, all coated samples show two newly appearing bands at wave numbers around 1354 cm^{-1} and 1595 cm^{-1}, which are highly characteristic for carbonaceous compounds. The feature located at 1354 cm^{-1} is assigned to the D band (disordered graphitic structure) and the one at 1595 cm^{-1} to the G band (graphitic structure) [9,20]. In general, carbon bands are much more intense than those of pristine ZFO. However, only for ZFO/Suc the characteristic ZFO bands do not appear anymore, while they can still be observed for ZFO/CA and ZFO/OLEA (inset in Fig. 2). Thus, it might be concluded that ZFO/Suc nanoparticles are homogenously coated by a carbonaceous film, whereas the other two samples are either partially coated or as for ZFO/OLEA, which contains a relatively low amount of carbon, the carbon coating is homogenous but rather thin. Nonetheless, all samples show comparable ratios of the D and G band intensities, indicating a similar degree of graphitization for the investigated carbon precursors [21].

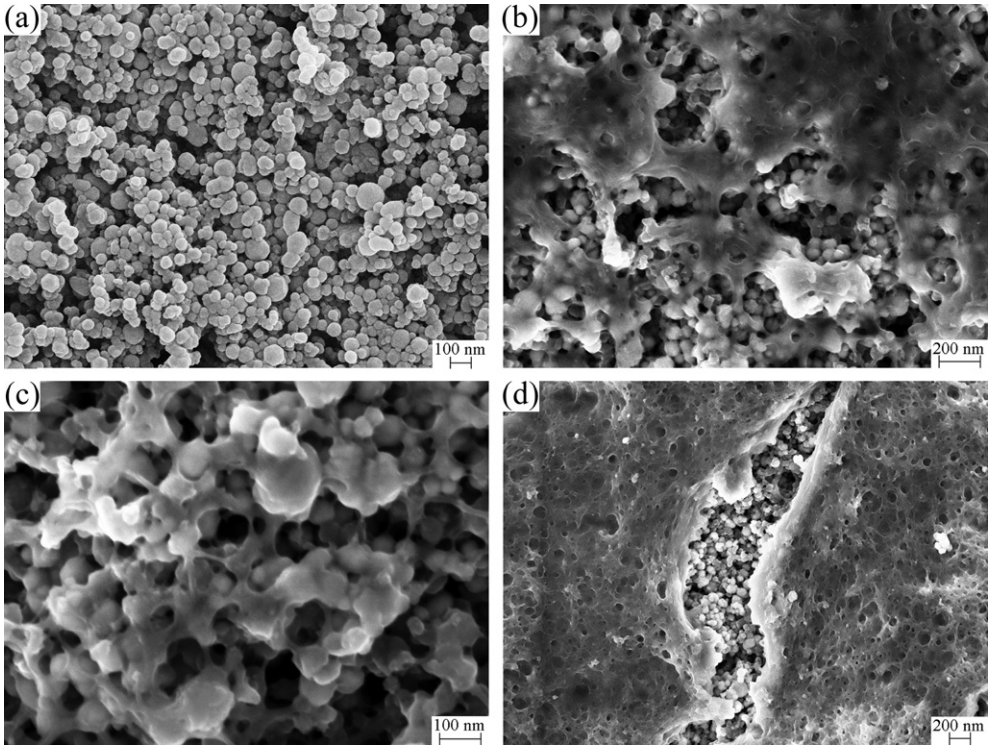

Fig. 5. SEM images of electrodes based on pristine ZFO: (a) freshly made electrode at a magnification of 100 k×; (b–d) electrode after 10 cycles at a magnification of (b) 50 k×, (c) 100 k×, and (d) 25 k×.

In order to gather further insights on the morphology of the three coated materials, SEM analysis was performed (Fig. 3). From the images it is obvious that pristine ZFO (Fig. 3a) and ZFO/Suc (Fig. 3b) have very similar particle size and shape, confirming the assumption of a homogenous carbon coating as revealed by Raman spectroscopy and previously shown by HRTEM analysis [8]. However, a slight particle aggregation is observed, which can be explained by the interconnection of the coated ZFO nanoparticles by carbon [8]. In Fig. 3c the ZFO/CA composite thermally treated at 400 °C is shown. It is obvious that the ZFO nanoparticles are highly agglomerated. Moreover, these ZFO agglomerates appear to be embedded in a carbon matrix rather than homogeneously coated. These observations are in line with the determined BET surface area of the corresponding samples listed in Table 1. A homogenous coating results in a higher specific surface area than bulky carbon. For ZFO/OLEA (Fig. 3d) no difference in particle shape and size was observed compared to the pristine sample. Again, this corresponds well with the determined BET surface area, which is very close to that of the pristine sample. However, the remaining carbon cannot be specifically located, strengthening the initial assumption, that the obtained carbon coating might be extremely thin rather than inhomogeneous.

Bearing in mind that the different composites show no significant difference in the ratio of the D and the G band intensity, the three composites and pristine ZFO were electrochemically investigated. The electrochemical investigation of pristine ZFO is presented in Fig. 4. In Fig. 4a the constant current cycling between 0.01 V and 3.0 V at C/10 rate (100 mA g^{-1}) of pristine ZFO is shown. As already described in literature the capacity fades rapidly upon cycling [8]. After 100 cycles the reversible specific capacity further decreased to 230 mAh g^{-1}, corresponding to a capacity retention of only 25%. The first cycle irreversible capacity loss (ICL) is 23%. In fact, this ICL is lower than previously reported values [3–5,7]. In Fig. 4b the potential profiles for the second and each 10th cycle are shown. The polarization of the electrode increases sharply upon cycling while the characteristic potential profile is slowly vanishing upon cycling. In Fig. 4c impedance spectra of a ZFO/Li cell after the 1st, 2nd, 3rd, 4th, 5th, and 10th cyclic potential sweep are presented. This continuous impedance increase upon cycling is generally assigned to the ongoing formation of a polymeric layer on the particles surface and a resulting gradual loss of electrical contact within the electrode [22]. Additionally, other factors such as, for instance, changes in porosity of the electrode upon cycling might have an influence on the charge transfer impedance. Nonetheless, the formation of a polymeric layer on the particle surface and moreover the formation of a thick film, covering the whole electrode is revealed by *ex situ* SEM analysis of a ZFO-based electrode after 10 cycles (Fig. 5a–d). The formation of such thick and likely electronically insulating layer on the electrode might also be a reason for the increasing polarization of the electrode upon continuous cycling as observed by means of galvanostatic cycling. The constant current cycling and the corresponding potential profiles of electrodes based on the ZFO/C composite materials are presented in Fig. 6. ZFO/Suc (Fig. 6a) shows an initial discharge capacity of 1440 mAh g^{-1} with a reversible (charge) capacity of 1050 mAh g^{-1}, corresponding to an ICL of 27%. Upon continuous (dis-)charging the specific capacity increases to around 1100 mAh g^{-1} after 60 cycles. The initial reversible capacity is higher than the reference value for pristine ZFO (916 mAh g^{-1}), which may be explained by the enhanced activation of the active material due to the increased electronic conductivity within the electrode and the improved electrolyte access resulting from the porous carbon coating. However, upon cycling it exceeds the theoretically expected limit. This behavior has already been reported for carbon coated $ZnFe_2O_4$ [8] as well as other transition metal oxides [23–28]. The reason for the increasing capacity upon cycling needs to be further investigated. However, the corresponding potential profiles reveal that this increase in capacity is

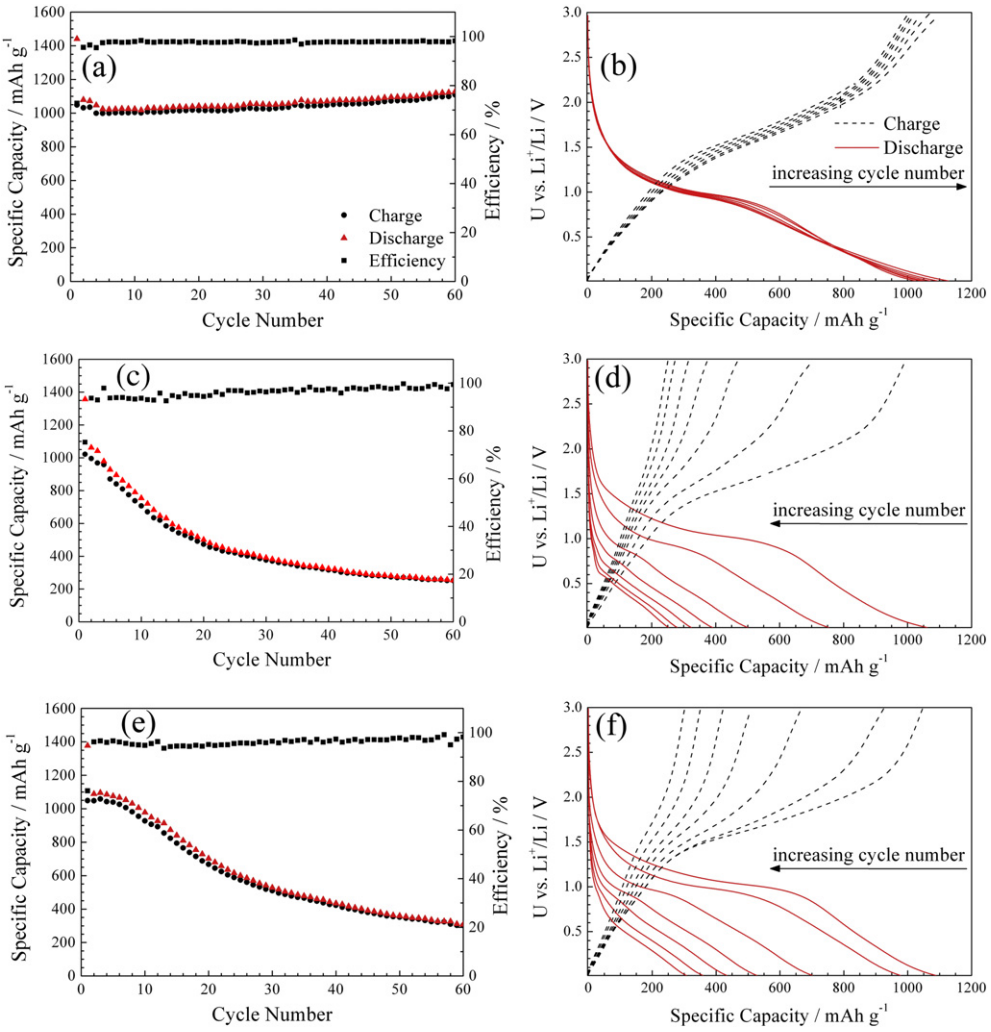

Fig. 6. Galvanostatic cycling of ZFO-based electrodes (a) ZFO/Suc, (c) ZFO/CA, and (e) ZFO/OLEA. Three formation cycles at C/20 (50 mA g^{-1}), followed by constant current cycling at C/10 (100 mA g^{-1}). Cut-off potentials: 0.01 V and 3.0 V. Potential profiles of the 2nd (C/20), 10th, 20th, 30th, 40th, 50th, and 60th cycle of ZFO-based electrodes (b) ZFO/Suc, (d) ZFO/CA, and (f) ZFO/OLEA. Cut-off potentials: 0.01 V and 3.0 V. Applied C rate: C/10 (100 mA g^{-1}).

mainly gained in a voltage region close to the lower cut-off potential of 0.01 V (Fig. 6b). Hence, it has been suggested, that this extra capacity originates from the conductive agent, the carbon coating, as well as the reversible formation of the polymeric layer [8]. In fact, future studies on this material, focusing on the optimization of the carbon coating obtained by using sucrose as carbon source and generally the carbon content, will hopefully allow further insight into this phenomenon. Nevertheless, in the case of ZFO/Suc the formation of such a polymeric layer does not have a detrimental effect on the internal resistance as revealed by the absence of an increasing electrode polarization (Fig. 6b). Overall, ZFO/Suc provides a highly stable long-term cycling performance.

For ZFO/CA an initial discharge capacity of 1360 mAh g^{-1} is observed, followed by an initial reversible capacity of 1020 mAh g^{-1}, resulting in an ICL of 25% (Fig. 6c). Concerning the long-term cycling stability, however, no significant improvement relatively to pristine ZFO was obtained. This poor cycling stability might have several reasons: The comprised phase impurities of ZnO and FeO as well as the lower carbon content relatively to ZFO/Suc and the formation of large aggregates of ZFO particles and carbon. However, the lack of an efficient percolating conductive network is revealed by a steadily increasing IR drop upon cycling (Fig. 6d). For ZFO/OLEA (Fig. 6e) a first cycle total and reversible capacity of

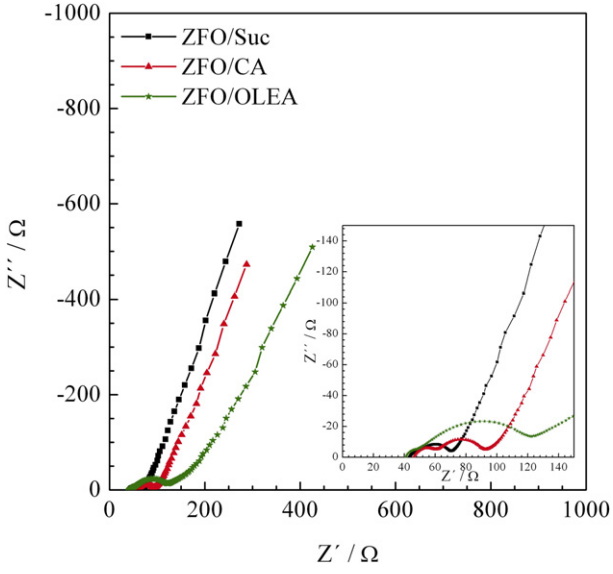

Fig. 7. Nyquist plots for ZFO/Suc, ZFO/CA, and ZFO/OLEA electrodes after ten cycles at a potential of 3.0 V.

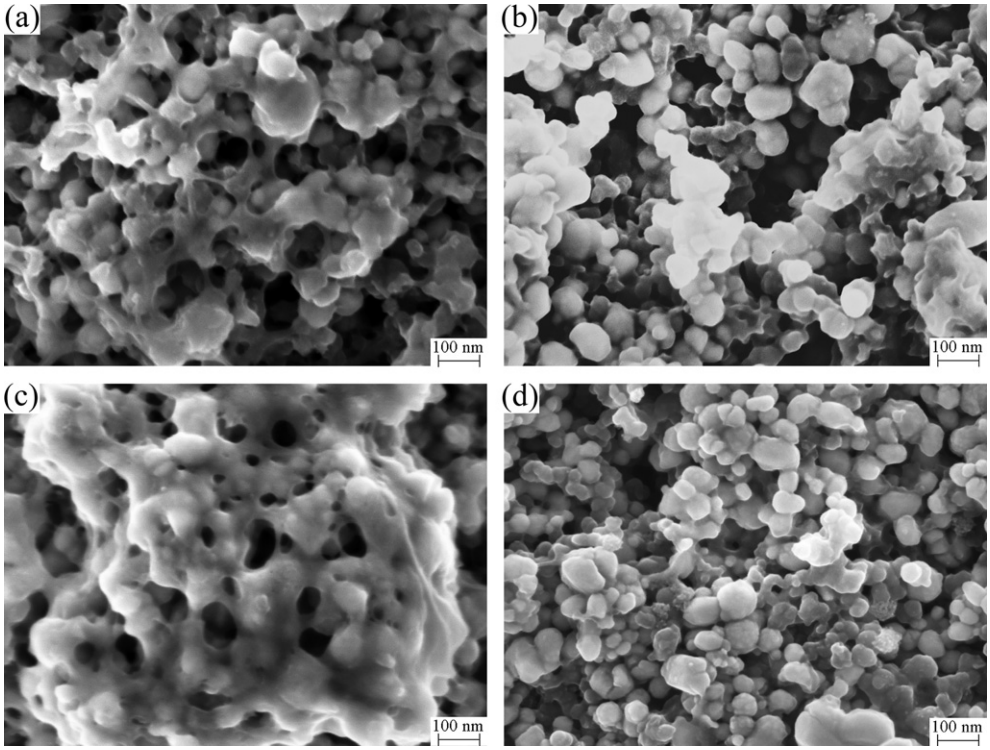

Fig. 8. SEM images of electrodes based on (a) pristine ZFO, (b) ZFO/Suc, (c) ZFO/CA, and (d) ZFO/OLEA after 10 cycles. Magnification: 100 k×.

1380 mAh g^{-1} and 1050 mAh g^{-1} were obtained, respectively, corresponding to an ICL of 24%. Comparing the ICL of all four samples it appears obvious that it is increasing in the same order as the BET surface area (ZFO/Suc > ZFO/CA > ZFO/OLEA > ZFO), which can be explained by an increased electrolyte decomposition for high surface area active materials and consequently, an increased SEI formation. However, the cycling stability of ZFO/OLEA was slightly improved, relatively to ZFO/CA, particularly for the first 5 cycles, although, once again, the capacity fades rather rapidly upon the subsequent cycles. Nevertheless, by comparing the potential profiles of ZFO/OLEA with those of ZFO/CA, it is obvious that a homogenous carbon distribution is much more efficient in decreasing the electrode polarization than a simple increase of the total carbon content (Fig. 6d and f). The shape of the potential *vs.* specific capacity curve is similar to that of pristine ZFO. Nevertheless, the capacity is, at least up to 60 cycles, higher, before eventually fading to the same level as pristine ZFO. Nonetheless, it can be stated that, even by a thin carbon coating, the electrode polarization growing upon cycling can be reduced (Fig. 6f) and therefore the electrochemical performance of ZFO, in terms of capacity *vs.* cycling can be improved. However, 2.2 wt.% of carbon do not permit a stable long-term cycling.

Electrochemical impedance spectroscopy was performed to investigate the effect of carbon coating on ZFO nanoparticles. The comparison of the impedance spectra of the ZFO/C composites after ten cyclic potential sweeps is presented in Fig. 7. The resistance of the electrodes increases in the order: ZFO/Suc, ZFO/CA, and ZFO/OLEA, i.e., in a reversed manner of the specific surface area (Table 1). These results show that the complete and homogenous carbon coating of ZFO/Suc offers a more efficient electronic conductive network than those of ZFO/OLEA, which is incomplete or very thin coated, and ZFO/CA, which is obviously not homogeneously coated. The increased surface area is due to the porous character of the carbon coating which allows an enhanced electrolyte penetration of the electrode composite, finally leading to an improved ionic conductivity in the electrode [8,29]. In Fig. 8(a–d) SEM images after 10 cycles are presented. For uncoated ZFO (Fig. 8a) and non-homogeneously carbon coated ZFO/CA (Fig. 8c) a layer on the electrode surface can be observed, whereas ZFO/Suc (Fig. 8b) and ZFO/OLEA (Fig. 8d) show a significantly decreased film formation upon cycling. These results are in line with the result obtained by means of galvanostatic cycling and the corresponding potential profiles.

4. Conclusions

The influence of sucrose, citric acid, and oleic acid on the realization of carbonaceous, electronically conductive networks incorporating $ZnFe_2O_4$ nanoparticles has been investigated. Sucrose turned out as the carbon precursor of choice for the improvement of the electrochemical performance of ZFO. The obtained coating showed a homogenous distribution, evenly covering the ZFO nanoparticles. Additionally, the increased BET surface area, allowing an increased electrolyte penetration of the electrode composite, led to a decreased resistance of the prepared electrodes compared to the pristine ZFO and the other ZFO/C composites. These properties finally led to an improved electrochemical performance in terms of a dramatically enhanced long-term cycling stability, confirming the beneficial effect of the carbon coating on the performance of $ZnFe_2O_4$ nanoparticles as active material for lithium-ion anodes.

In particular, it was revealed that the homogeneity of such a coating rather than the overall carbon amount plays a key-role. Accordingly, carbon coated $ZnFe_2O_4$ nanoparticles utilizing sucrose as carbon precursor, which offers the best coating homogeneity while, at the same time, allowing a facile processing, showed excellent electrochemical performance delivering a specific capacity higher than 1000 mAh g^{-1} for more than 60 cycles.

Acknowledgments

Financial support from the European Commission in the ORION project (229036) under the Seventh Framework Programme (7th FWP) is gratefully acknowledged. Furthermore, the authors want to thank Mr. Sebastian Menne and Mr. Steffen Krueger for performing SEM analysis.

References

[1] Y. Nishi, Chem. Rec. 1 (2001) 406–413.
[2] B. Scrosati, J. Garche, J. Power Sources 195 (2010) 2419–2430.
[3] Y. Sharma, N. Sharma, G.V.S. Rao, B.V.R. Chowdari, Electrochim. Acta 53 (2008) 2380–2385.
[4] X.W. Guo, X. Lu, X.P. Fang, Y. Mao, Z.X. Wang, L.Q. Chen, X.X. Xu, H. Yang, Y.N. Liu, Electrochem. Commun. 12 (2010) 847–850.
[5] Y.F. Deng, Q.M. Zhang, S.D. Tang, L.T. Zhang, S.N. Deng, Z.C. Shi, G.H. Chen, Chem. Commun. 47 (2011) 6828–6830.
[6] P.F. Teh, Y. Sharma, S.S. Pramana, M. Srinivasan, J. Mater. Chem. 21 (2011) 14999–15008.
[7] Y. Ding, Y.F. Yang, H.X. Shao, Electrochim. Acta 56 (2011) 9433–9438.
[8] D. Bresser, E. Paillard, R. Kloepsch, M. Fiedler, S. Krueger, R. Schmitz, M. Winter, S. Passerini, Adv. Energy Mater. (2012), http://dx.doi.org/10.1002/aenm.201200735.
[9] X.B. Hu, Z.J. Lin, K.R. Yang, Y.J. Huai, Z.H. Deng, Electrochim. Acta 56 (2011) 5046–5053.
[10] R. Dominko, M. Bele, M. Gaberscek, M. Remskar, D. Hanzel, S. Pejovnik, J. Jamnik, J. Electrochem. Soc. 152 (2005) A607–A610.
[11] Y. Kadoma, J.M. Kim, K. Abiko, K. Ohtsuki, K. Ui, N. Kumagai, Electrochim. Acta 55 (2010) 1034–1041.
[12] Y.D. Cho, G.T.K. Fey, H.M. Kao, J. Power Sources 189 (2009) 256–262.
[13] M.M. Doeff, J.D. Wilcox, R. Kostecki, G. Lau, J. Power Sources 163 (2006) 180–184.
[14] Y.H. Nien, J.R. Carey, J.S. Chen, J. Power Sources 193 (2009) 822–827.
[15] D. Bresser, E. Paillard, E. Binetti, S. Krueger, M. Striccoli, M. Winter, S. Passerini, J. Power Sources 206 (2012) 301–309.
[16] M. Armand, M. Gauthier, J.F. Magnan, N. Ravet, US Patent, US 7,285,260 B2.
[17] J. Moskon, R. Dominko, R. Cerc-Korosec, M. Gaberscek, J. Jamnik, J. Power Sources 174 (2007) 683–688.
[18] P.D. Cozzoli, A. Kornowski, H. Weller, J. Am. Chem. Soc. 125 (2003) 14539–14548.
[19] S. Ayyappan, G. Paneerselvam, M.P. Antony, J. Philip, Mater. Chem. Phys. 128 (2011) 400–404.
[20] R. Baddour-Hadjean, J.P. Pereira-Ramos, Chem. Rev. 110 (2010) 1278–1319.
[21] T. Yuan, X. Yu, R. Cai, Y.K. Zhou, Z.P. Shao, J. Power Sources 195 (2010) 4997–5004.
[22] J. Vetter, P. Novak, M.R. Wagner, C. Veit, K.C. Moller, J.O. Besenhard, M. Winter, M. Wohlfahrt-Mehrens, C. Vogler, A. Hammouche, J. Power Sources 147 (2005) 269–281.
[23] F. Badway, I. Plitz, S. Grugeon, S. Laruelle, M. Dolle, A.S. Gozdz, J.M. Tarascon, Electrochem. Solid State Lett. 5 (2002) A115–A118.
[24] P. Poizot, S. Laruelle, S. Grugeon, L. Dupont, J.M. Tarascon, Nature 407 (2000) 496–499.
[25] S. Grugeon, S. Laruelle, L. Dupont, J.M. Tarascon, Solid State Sci. 5 (2003) 895–904.
[26] J. Li, H.M. Dahn, L.J. Krause, D.B. Le, J.R. Dahn, J. Electrochem. Soc. 155 (2008) A812–A816.
[27] G.M. Zhou, D.W. Wang, F. Li, L.L. Zhang, N. Li, Z.S. Wu, L. Wen, G.Q. Lu, H.M. Cheng, Chem. Mater. 22 (2010) 5306–5313.
[28] K.M. Shaju, F. Jiao, A. Debart, P.G. Bruce, Phys. Chem. Chem. Phys. 9 (2007) 1837–1842.
[29] A. Gibaud, J.S. Xue, J.R. Dahn, Carbon 34 (1996) 499–503.